

THE REDSHIFT EVOLUTION OF THE 2 – 8 KEV X-RAY LUMINOSITY FUNCTION

L. L. COWIE,¹ A. J. BARGER,^{2,3,1} M. W. BAUTZ,⁴ W. N. BRANDT,⁵ G. P. GARMIRE⁵

To appear in The Astrophysical Journal Letters

ABSTRACT

The high angular resolution and sensitivity of the *Chandra X-ray Observatory* has yielded large numbers of faint X-ray sources with measured redshifts in the soft (0.5 – 2 keV) and hard (2 – 8 keV) energy bands. Many of these sources show few obvious optical signatures of active galactic nuclei (AGN). We use *Chandra* observations of the Hubble Deep Field North region, A370, and the Hawaii Survey Fields SSA13 and SSA22, together with the *ROSAT* Ultra Deep Survey soft sample and the *ASCA* Large Sky Survey hard sample, to construct rest-frame 2 – 8 keV luminosity functions versus redshift for all the X-ray sources, regardless of their optical AGN characteristics. At $z = 0.1 - 1$ most of the 2 – 8 keV light density arises in sources with luminosities in the 10^{42} ergs s^{-1} to 10^{44} ergs s^{-1} range. We show that the number density of sources in this luminosity range is rising, or is at least constant, with decreasing redshift. Broad-line AGN are the dominant population at higher luminosities, and these sources show the well-known rapid positive evolution with increasing redshift to $z \sim 3$. We argue that the dominant supermassive black hole formation has occurred at recent times in objects with low accretion mass flow rates rather than at earlier times in more X-ray luminous objects with high accretion mass flow rates.

Subject headings: cosmology: observations — galaxies: evolution — galaxies: formation — galaxies: active

1. INTRODUCTION

Hard X-ray surveys provide the most direct probe of supermassive black hole (SMBH) accretion activity, since high energy X-rays can penetrate extremely large column densities of gas and dust. Early analyses of deep *Chandra* X-ray surveys found that optical selections of active galactic nuclei (AGN) had missed large numbers of accreting SMBHs. Barger et al. (2001b) showed that the redshift history of SMBH growth is more strongly peaked to low redshifts than had been inferred from optically-selected samples.

With the high spatial resolution and energy sensitivity of deep *Chandra* observations, X-ray samples can be selected at both low and high redshifts in the same rest-frame *hard* energy band and their optical counterparts, and hence spectroscopic redshifts ($\sim 65\%$ can be identified), unambiguously determined. The hardest band for which the hard X-ray luminosity function (HXLf) can presently be determined over a wide range of redshifts is rest-frame 2 – 8 keV. Although some Compton-thick sources may still be omitted, the accounting will be far more complete than that of any other available sample.

In this paper we use the 1 Ms exposure of the *Chandra* Deep Field North (CDF-N) and three ~ 100 Ks exposures of the A370, SSA13, and SSA22 fields, together with previous *ROSAT* and *ASCA* data, to construct the rest-frame 2 – 8 keV luminosity function from $z = 0$ to 4 and model the SMBH accretion history. We assume $\Omega_M = 1/3$, $\Omega_\Lambda = 2/3$, and $H_o = 65$ km s^{-1} Mpc $^{-1}$. We use L_x to denote the rest-frame 2 – 8 keV luminosity.

2. X-RAY SAMPLE SELECTION

The faintest data are taken from the 1 Ms CDF-N catalogs of Brandt et al. (2001; hereafter B01) and Barger et al. (2002). We exclude known stars and the small number of extended X-ray sources. The flux limits are $\approx 3 \times 10^{-17}$ ergs cm^{-2} s^{-1} (0.5 – 2 keV) and $\approx 2 \times 10^{-16}$ ergs cm^{-2} s^{-1} (2 – 8 keV). Below a flux of 1.6×10^{-14} ergs cm^{-2} s^{-1} (2 – 8 keV) and 6×10^{-15} ergs cm^{-2} s^{-1} (0.5 – 2 keV) we include only sources lying within $8'$ of the aimpoint where the redshift identifications are most complete; above these fluxes we include all the sources. This restricted sample contains 199 (52%) sources in the 2 – 8 keV band and 219 (57%) in the 0.5 – 2 keV band, where the parentheses are the percentages with redshifts. We supplement the sample at fluxes above 2×10^{-15} ergs cm^{-2} s^{-1} (2 – 8 keV) and 3×10^{-16} ergs cm^{-2} s^{-1} (0.5 – 2 keV) with data from the SSA13 field (Barger et al. 2001a), the A370 field (Barger et al. 2001b), and the SSA22 field (A. J. Barger et al., in preparation). This adds a further 67 (72%) sources in the 2 – 8 keV band and 88 (60%) in the 0.5 – 2 keV band. We further supplement the sample with the larger area bright flux samples in the soft band from *ROSAT* (Lehmann et al. 2001) and the hard band from *ASCA* (Akiyama et al. 2000). These have highly complete spectroscopic identifications.

For the conversion of counts to flux in the CDF-N, we use the X-ray spectral photon indices Γ determined in B01 from the hard-band to soft-band counts ratios. For the conversions in the remaining *Chandra* fields, we assume a fixed $\Gamma = 1.2$, which is approximately the average Γ in

¹Institute for Astronomy, University of Hawaii, 2680 Woodlawn Drive, Honolulu, Hawaii 96822

²Department of Astronomy, University of Wisconsin-Madison, 475 North Charter Street, Madison, WI 53706

³Department of Physics and Astronomy, University of Hawaii, 2505 Correa Road, Honolulu, HI 96822

⁴Center for Space Research, Massachusetts Institute of Technology, Cambridge, MA 02139

⁵Department of Astronomy & Astrophysics, 525 Davey Laboratory, The Pennsylvania State University, University Park, PA 16802

the B01 sample. For the flux conversions in the *ROSAT* and *ASCA* samples, we use the softer Γ values assumed by Lehmann et al. (2001) and Akiyama et al. (2000), which are appropriate for higher flux sources.

We determined the solid angle covered by the sample at a given flux by comparing the observed numbers of objects as a function of flux with the measured number counts in the appropriate energy band. For 2 – 8 keV we use the averaged counts given in Cowie et al. (2002), and for 0.5 – 2 keV we use the power-law fits of Mushotzky et al. (2000), which agree with other determinations (e.g., B01; Rosati et al. 2002). The solid angle covered by the combined 2 – 8 keV samples ranges from just under 0.01 deg² at the faintest fluxes to 5.8 deg² at the highest fluxes. At 10^{-14} ergs cm⁻² s⁻¹ (2 – 8 keV) the solid angle is 0.11 deg². The maximum solid angle covered by the combined 0.5 – 2 keV samples is 0.42 deg². At 10^{-15} ergs cm⁻² s⁻¹ (0.5 – 2 keV) the solid angle is 0.12 deg².

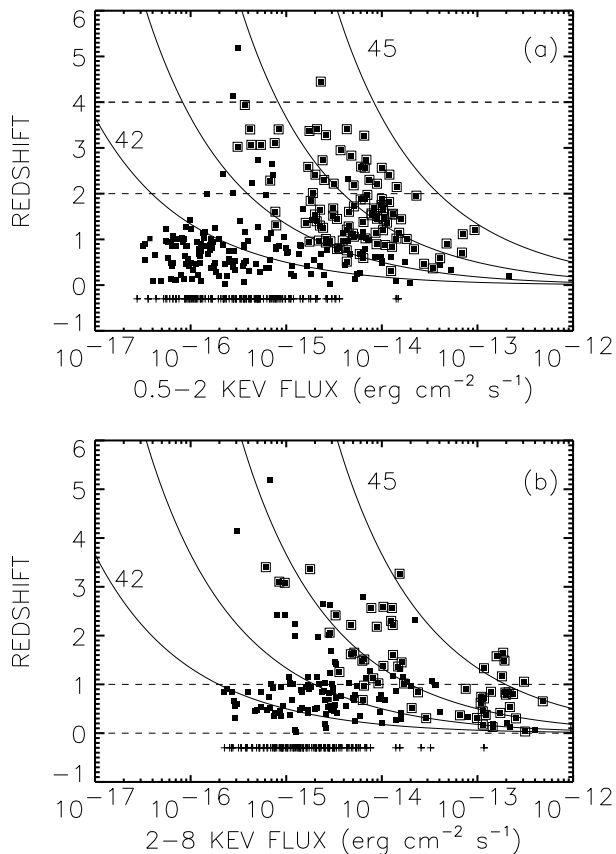


FIG. 1.— Redshift versus flux for sources selected in (a) the 0.5–2 keV band and (b) the 2–8 keV band. Solid curves show flux versus redshift for sources with $L_x = 10^{42}$ ergs s⁻¹ (lowest curve), 10^{43} ergs s⁻¹, 10^{44} ergs s⁻¹, and 10^{45} ergs s⁻¹ (highest curve), computed with a K -correction for a $\Gamma = 1.8$ power-law spectrum. Dashed lines show the redshift intervals used in constructing the HXLFs. Sources with broad-line optical spectra are enclosed in a second, larger symbol. Spectroscopically unidentified sources are denoted by plus signs at $z = -0.3$.

In Fig. 1a and b we show redshift versus flux for the soft and hard selected samples, respectively, including sources that have not been spectroscopically identified. The solid curves correspond to loci of constant L_x . Sources with broad-line optical/UV spectra are denoted

by a second, larger symbol. Any source more luminous than 10^{42} ergs s⁻¹ is very likely an AGN on energetic grounds (Zezas, Georgantopoulos, & Ward 1998; Moran et al. 1999), though many of the intermediate luminosity sources do not show obvious AGN signatures in the optical. It is clear from Fig. 1 that the highest X-ray luminosity sources are mostly broad-line AGN.

3. EVOLUTION OF THE AGN X-RAY LUMINOSITY FUNCTION

In the present section we concentrate on two redshift intervals: $z = 0.1 - 1$, as shown by the dashed lines in Fig. 1b, and $z = 2 - 4$, as shown in Fig. 1a. With these redshift intervals we can compare samples chosen in approximately the same rest-frame hard X-ray energy range of 3 – 12 keV (the observed 2 – 8 keV band at the center of the low redshift interval) and 2 – 8 keV (the observed 0.5 – 2 keV band at the center of the high redshift interval). The remaining small differential K -corrections to rest-frame 2 – 8 keV are made by assuming that the spectra can be approximated by $\Gamma = 1.8$ power-laws. We have chosen to use this spectral index since the differential K correction is mostly significant in correcting from higher to lower energies where the spectra may be better represented by the unabsorbed intrinsic power law (see Barger et al. 2002). However, the results are only weakly sensitive to this assumption. For a $\Gamma = 1.2$ power-law K -correction the HXLF at $z = 2 - 4$ is essentially unchanged while the HXLFs at $z = 0.1 - 1$ shifts to slightly lower luminosities (a factor of 1.27) while the shape remains approximately the same.

We have chosen not to correct for the intrinsic absorption since this too requires an assumption about the intrinsic spectrum and also about the form of the absorption and any scattering. Since we are comparing in the same rest frame at different redshifts this will not affect the HXLF comparison unless there is substantial evolution in the intrinsic absorption. Moreover in the 2 – 8 keV rest frame band the average absorption corrections are not very large. If we assume an intrinsic spectral index of $\Gamma = 1.8$ and a simple photoelectric absorption the average absorption correction to L_x is 1.14 in the 0.1 – 1 redshift range and 1.53 in the $z = 2 - 4$ range.

We probe to an L_x below 10^{43} ergs s⁻¹ in the high redshift interval and below 10^{42} ergs s⁻¹ in the low redshift interval. Both samples are highly complete in redshift identifications at high luminosities. At $L_x > 10^{44}$ ergs s⁻¹ in the high redshift interval there are 22 spectroscopically identified sources, 21 of which are broad-line AGN. At most there are a further 18 spectroscopically unidentified sources that could lie at these luminosities in this redshift interval; however, a substantial fraction of these are likely at other redshifts. At $L_x > 10^{44}$ ergs s⁻¹ in the low redshift interval, 85% of the identified sources are broad-line AGN, and there are only three unidentified sources that could lie at these luminosities in this redshift interval. Thus, most of the high luminosity X-ray sources are broad-line AGN rather than obscured AGN.

The differential HXLF as a function of X-ray luminosity and redshift, $d\Phi(L_x, z)/d\log L_x$, is the number of X-ray sources per unit comoving volume per unit logarithmic luminosity. We adopt the $1/V_a$ method to estimate the

binned HXLF in different redshift shells as

$$\frac{d\Phi}{d\log L_x} = \frac{\sum_i 1/V_a^i}{\Delta \log L_x}, \quad (1)$$

where the V_a^i is the total comoving volume in the redshift bin Δz in which source i with luminosity L_x could lie and still be included in the sample and the summation is over all sources in the given redshift interval and luminosity bin. (Log denotes the base 10 logarithm.)

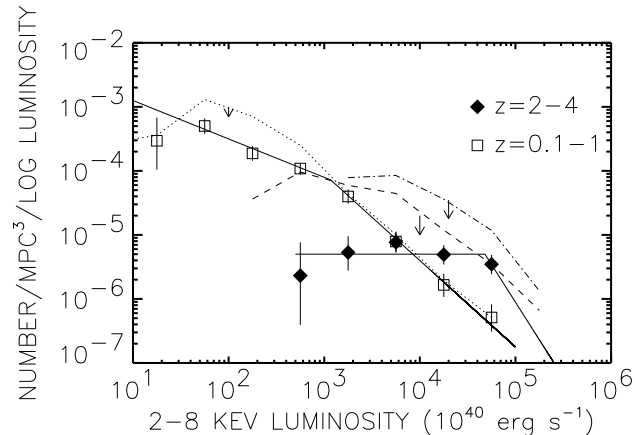


FIG. 2.— Rest-frame 2–8 keV luminosity function per unit logarithmic luminosity in the redshift intervals $z = 0.1-1$ (open squares) and $z = 2-4$ (solid diamonds). In the $z = 0.1-1$ ($z = 2-4$) interval the HXLF was computed from observed-frame 2–8 keV ($0.5-2$ keV). An intrinsic $\Gamma = 1.8$ was assumed, for which there is only a small differential K -correction to rest-frame 2–8 keV. Poissonian 1σ uncertainties are based on the number of sources in each luminosity bin. Dotted ($z = 0.1-1$) and dashed ($z = 2-4$) lines are maximal HXLFs found by assigning all the spectroscopically unidentified sources to the center of each redshift interval. Dot-dashed line is an upper bound on the $z = 2-4$ HXLF obtained by selecting in observed-frame 2–8 keV and then assigning all the unidentified sources to this redshift interval. Solid lines show a broken power-law fit to the low redshift HXLF with a slope of -0.6 below 1.2×10^{43} ergs s^{-1} and -1.35 above, and to the high redshift HXLF with a slope of 0.0 below 4.8×10^{44} ergs s^{-1} and -2.35 above. The upper L_x fit in the high redshift interval is based on the HXLF of Miyaji et al. (2001) shown in Fig. 3.

Our measured HXLFs for the two redshift intervals are shown in Fig. 2 with Poissonian 1σ uncertainties based on the number of galaxies in each luminosity bin. However, since incompleteness is a potentially larger source of error, we recomputed the HXLFs by assigning all the spectroscopically unidentified sources to the center of each redshift interval (i.e., we included all the unidentified sources in both redshift intervals). Dotted ($z = 0.1-1$) and dashed ($z = 2-4$) lines in Fig. 2 show these maximal limits. Because the spectroscopic identifications are much more complete at the high X-ray fluxes, the associated systematic uncertainties are larger at lower L_x . In principle photometric redshifts can be estimated for the sources, and at higher redshifts this procedure is effective (A. J. Barger et al., in preparation). However, over the $z = 0-4$ range there could be considerable uncertainties in assigning photometric redshifts to sources with substantial AGN contributions, so we prefer our more conservative approach. Analyses of the HXLF using alternate techniques suggest that the lowest luminosity point in the determinations may be biased low (e.g. Page and Carrera 2000, Miyaji et al. 2001) but the effect is small compared to the statistical and systematic uncertainties.

At $L_x > 10^{44}$ ergs s^{-1} Fig. 2 shows the familiar rise of the number counts with redshift. These counts are dominated by broad-line AGN. However, at lower L_x the $z = 0.1-1$ counts lie above the $z = 2-4$ counts, or are comparable if we use the maximal correction for incompleteness. Since it is extremely unlikely that all the unidentified sources lie in the $z = 2-4$ range (this would result in a large deficiency at $z = 1-2$), the present-day number density of sources at $L_x \sim 10^{43}$ ergs s^{-1} is higher than it was in the past. This result cannot be significantly changed by highly obscured sources: the dot-dashed line shows the upper bound on the $z = 2-4$ HXLF if we selected in observed-frame 2–8 keV, which corresponds to rest-frame 8–32 keV, and placed all the unidentified sources in this redshift interval. The resulting upper limit is a factor of ~ 2 higher than the upper limit obtained from the observed-frame 0.5–2 keV selection.

All the X-ray sources are included in Fig. 2 without regard to optical spectroscopic classification. Previous HXLF analyses have generally focused on broad-line AGN where the counterparts can be determined even in low resolution X-ray data (e.g., Boyle et al. 1998). To make a direct comparison with these earlier studies, in Fig. 3 we plot our spectroscopically identified broad-line AGN HXLFs in the intervals $z = 0.1-1$ and $z = 2-4$ with those derived by La Franca et al. (2002; $z = 0.5$) from *BeppoSAX* data and by Miyaji et al. (2001; $z = 2-4$) from *ROSAT* data. Our HXLFs agree with these brighter HXLFs in the overlap region where there is also some overlap in the datasets used. At $L_x \sim 10^{43}$ ergs s^{-1} there is little apparent evolution in the broad-line AGN HXLF, while at higher luminosities the HXLF increases with redshift.

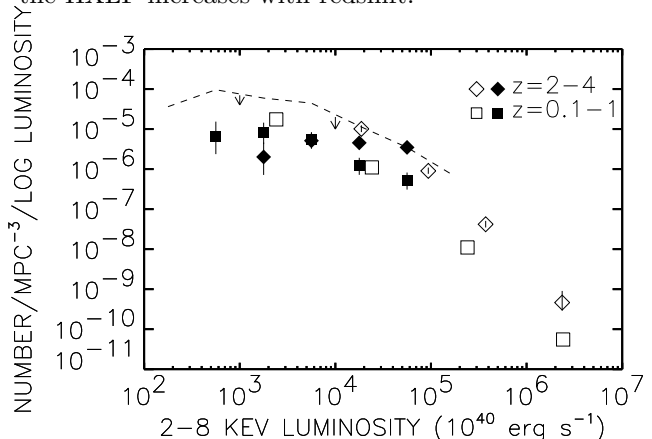


FIG. 3.— Rest-frame 2–8 keV broad-line AGN luminosity function per unit logarithmic luminosity in the redshift intervals $z = 0.1-1$ (solid squares) and $z = 2-4$ (solid diamonds). Dashed line is the maximal HXLF in the $z = 2-4$ interval found by assigning all the spectroscopically unidentified sources to the center of the interval. However, we expect that most of the broad-line AGN have been identified since they are optically bright and straightforward to identify spectroscopically. Open boxes (open diamonds) show the broad-line AGN HXLF at $z = 0.5$ ($z = 2-4$) derived by La Franca et al. (2002) (Miyaji et al. 2001).

4. COSMIC EVOLUTION

In Fig. 4a we show the comoving number density evolution with redshift of $L_x > 10^{42}$ ergs s^{-1} sources. At these luminosities the probability that the X-ray sources are powered by anything other than AGN is extremely

low, so we are mapping the evolution of intermediate luminosity AGN. In the $z = 1 - 2$ redshift bin we show the number densities from both observed-frame 2 – 8 keV (open squares) and observed-frame 0.5 – 2 keV (solid diamonds); the results are similar, although the soft band may be missing some obscured sources. The solid (2 – 8 keV) and dotted (0.5 – 2 keV) horizontal bars show the number densities obtained if all the spectroscopically unidentified sources are assigned redshifts at the center of each redshift bin. The bars are not consistent with one another because all the unidentified sources are included in all the bins.

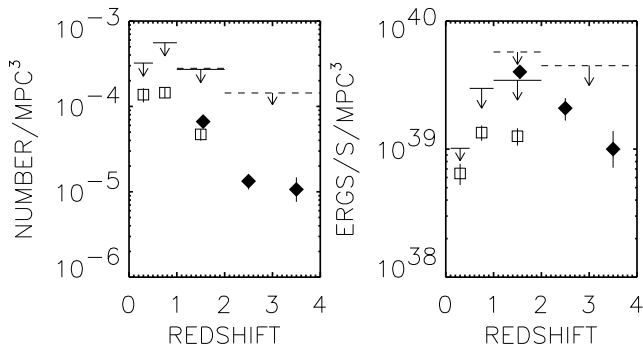


FIG. 4.— Evolution with redshift of the comoving number density (a) and the 2 – 8 keV comoving luminosity density production rate of $L_x > 10^{42}$ ergs s $^{-1}$ sources (b). Open squares (solid diamonds) are measured from observed-frame 2 – 8 keV (0.5 – 2 keV). Poissonian 1σ uncertainties are based on the number of sources in each bin. Dashed (0.5 – 2 keV) and solid (2 – 8 keV) bars show upper limits found by assigning all the unidentified sources to the center of each redshift bin, so the bars are not consistent with one another. To minimize this effect at high redshifts, we use a single $z = 2 - 4$ redshift bin. At the highest redshifts a small correction (less than 20%) has been applied to extrapolate from the minimum measured luminosity to $L_x = 10^{42}$ ergs s $^{-1}$. Note that the uncertainty in the $\dot{\lambda}_x$, which is weighted to higher luminosity sources, is smaller than the uncertainty in the number density.

The number density of intermediate luminosity AGN does not rise rapidly from $z \sim 0$ to $z \sim 2.5 - 3$, in contrast to that of higher luminosity AGN (e.g., Miyaji et al. 2000). In fact, the evolution with increasing redshift is flat or declining. Thus, AGN traced by X-ray luminosity show their own version of downsizing, just as star-forming galaxies do (Cowie et al. 1996). High X-ray luminosity sources, which strongly overlap with broad-line AGN (quasar) populations, peak at higher redshifts, while intermediate luminosity sources are still common now.

In Fig 4b we show the evolution with redshift of the 2 – 8 keV comoving luminosity density production rate of $L_x > 10^{42}$ ergs s $^{-1}$ sources ($\dot{\lambda}_x$). Integration of the power-law fits to the HXLFs shown in Fig. 2 give a similar answer: 1.9×10^{39} ergs s $^{-1}$ Mpc $^{-3}$ in the $z = 0.1 - 1$ redshift interval and 2.2×10^{39} ergs s $^{-1}$ Mpc $^{-3}$ in the $z = 2 - 4$ interval. The largest uncertainty is the redshift distribution of the unidentified sources rather than the small effects of extrapolation outside our observed luminosity range. This incompleteness uncertainty is less than a factor of 2.9 even in the high redshift interval (Fig. 4b).

We parameterize the evolution of $\dot{\lambda}_x$ as

$$\dot{\lambda}_x = A \left(\frac{1+z}{1.5} \right)^\alpha, \quad (2)$$

where α ranges from -0.4 (all unidentified sources in the low redshift interval) to 1.1 (all unidentified sources in the high redshift interval). If only identified sources are included, $\dot{\lambda}_x$ is roughly flat until the lowest $z = 0.1 - 0.5$ interval in Fig. 4 where it may drop slightly and $A \approx 2 \times 10^{39}$ ergs s $^{-1}$ Mpc $^{-3}$. Thus, the 2 – 8 keV luminosity density production rate evolves slowly with redshift, as was first noted in Barger et al. (2001b).

The SMBH accretion rate density is now given by

$$\dot{\rho}_{SMBH} = B \frac{\dot{\lambda}_x (1 - \epsilon)}{\epsilon c^2}, \quad (3)$$

where B is the correction from L_x to the bolometric luminosity of the AGN, and ϵ is the radiative efficiency of the accretion flow. Setting $B \sim 40$, which seems to be roughly valid for both unobscured and obscured AGN (Elvis et al. 1994; Barger et al. 2001b), and $\epsilon \sim 0.1$, which is close to the maximum possible radiative efficiency,

$$\dot{\rho}_{SMBH} = C \left(\frac{1+z}{1.5} \right)^\alpha, \quad (4)$$

where $C \approx 1.3 \times 10^{-5}$ M $_\odot$ yr $^{-1}$ Mpc $^{-3}$. Even within the uncertainty in α , SMBH growth is continuing strongly to the present time. Integrating Eq. 4 for $\alpha = 0$ gives a present universal SMBH density of $\approx 2 \times 10^5$ M $_\odot$ Mpc $^{-3}$, comparable to the $\approx 2 - 4 \times 10^5$ M $_\odot$ Mpc $^{-3}$ measured from local galaxies (Ferrarese & Merritt 2000; Gebhardt et al. 2000; Yu & Tremaine 2002). The late formation of the X-ray background reduces the required local SBMH mass density of previous estimates that assumed the bulk of the production was earlier (Fabian and Iwasawa 1999).

In summary, our results show that while the higher accretion mass flow rates that power the most luminous AGN peaked at higher redshift and are now much rarer, lower accretion mass flow rates are still common at the present time. These less luminous events dominate SMBH formation. The longer duration of the lower mass flow rate systems provide constraints on theoretical modelling of the SMBH formation (e.g., Haehnelt, Natarajan, & Rees 1998; Haiman & Menou 2000; Yu & Tremaine 2002) and on the evolution of the accretion disks feeding the sources, which may evolve more rapidly if they are initially of higher mass (Duschl 2002, private communication).

Support came from CXC grants DF1-2001X and GO2-3187B (LLC), NSF grants AST-0084816 (LLC) and AST-0084847 (AJB), the University of Wisconsin Research Committee with funds granted by the Wisconsin Alumni Research Foundation (AJB), the Alfred P. Sloan foundation (AJB), NSF CAREER award AST-9983783 (WNB), and NASA grant NAS 8-01128 (GPG, PI).

REFERENCES

- Akiyama, M., et al. 2000, *ApJ*, 532, 700
- Barger, A. J., Cowie, L. L., Mushotzky, R. F., & Richards, E. A. 2001a, *AJ*, 121, 662
- Barger, A. J., Cowie, L. L., Bautz, M. W., Brandt, W. N., Garmire, G. P., Hornschemeier, A. E., Ivison, R. J., & Owen, F. N. 2001b, *AJ*, 122, 2177
- Barger, A. J., Cowie, L. L., Brandt, W. N., Capak, P., Garmire, G. P., Hornschemeier, A. E., Steffen, A. T., & Wehner, E. H. 2002, 124, 1839
- Boyle, B. J., Georgantopoulos, I., Blair, A. J., Stewart, G. C., Griffiths, R. E., Shanks, T., Gunn, K. F., & Almaini, O. 1998, *MNRAS*, 296, 1
- Brandt, W. N., et al. 2001, *AJ*, 122, 2810 (B01)
- Cowie, L. L., Songaila, A., Hu, E. M., & Cohen, J. G. 1996, *AJ*, 112, 839
- Cowie, L. L., Garmire, G. P., Bautz, M. W., Barger, A. J., Brandt, W. N., & Hornschemeier, A. E. 2002, *ApJ*, 566, L5
- Elvis, M., et al. 1994, *ApJS*, 95, 1
- Fabian, A. & Iwasawa, K. 1999, *MNRAS*, 303, 34
- Ferrarese, L. & Merritt, D. 2000, *ApJ*, 539, L9
- Gebhardt, K., et al. 2000, *ApJ*, 539, L13
- Haehnelt, M. G., Natarajan, P., & Rees, M. J. 1998, *MNRAS*, 300, 817
- Haiman, Z. & Menou, K. 2000, *ApJ*, 531, 42
- La Franca, F., et al. 2002, *ApJ*, 570, 100
- Lehmann, I., et al. 2001, *A&A*, 371, 833
- Miyaji, T., Hasinger, G., & Schmidt, M. 2000, *A&A*, 353, 25
- Miyaji, T., Hasinger, G., & Schmidt, M. 2001, *A&A*, 369, 49
- Moran, E. C., Lehnert, M. D., & Helfand, D. J. 1999, *ApJ*, 526, 649
- Mushotzky, R. F., Cowie, L. L., Barger, A. J., & Arnaud, K. A. 2000, *Nature*, 404, 459
- Page, M. J., & Carrera, F. J. 2000, *MNRAS*, 311, 433
- Rosati, P., et al. 2002, *ApJ*, 566, 667
- Yu, Q. & Tremaine, S. 2002, *MNRAS*, 335, 965
- Zezas, A., Georgantopoulos, I., & Ward, M. J. 1998, *MNRAS*, 301, 915